






A single factor elicits multilineage reprogramming of astrocytes in the adult mouse striatum

Yunjia Zhang^{a,b,1}, Boxun Li^{c,d,e,1} , Sergio Cananzi^{a,b}, Chuanhui Han^f, Lei-Lei Wang^{a,b}, Yuhua Zou^{a,b}, Yang-Xin Fu^f , Gary C. Hon^{b,c,d,e,2} , and Chun-Li Zhang^{a,b,2}

Edited by Arnold Kriegstein, University of California, San Francisco, CA; received April 21, 2021; accepted January 24, 2022 by Editorial Board Member Nancy Y. Ip

Astrocytes in the adult brain show cellular plasticity; however, whether they have the potential to generate multiple lineages remains unclear. Here, we perform in vivo screens and identify DLX2 as a transcription factor that can unleash the multipotentiality of adult resident astrocytes. Genetic lineage tracing and time-course analyses reveal that DLX2 enables astrocytes to rapidly become ASCL1⁺ neural progenitor cells, which give rise to neurons, astrocytes, and oligodendrocytes in the adult mouse striatum. Single-cell transcriptomics and pseudotime trajectories further confirm a neural stem cell-like behavior of reprogrammed astrocytes, transitioning from quiescence to activation, proliferation, and neurogenesis. Gene regulatory networks and mouse genetics identify and confirm key nodes mediating DLX2-dependent fate reprogramming. These include activation of endogenous DLX family transcription factors and suppression of Notch signaling. Such reprogramming-induced multipotency of resident glial cells may be exploited for neural regeneration.

in vivo reprogramming | induced neural progenitor cells | astrocytes | DLX2 | scRNA-seq

During neural development, multipotent neural stem cells (NSCs) sequentially generate neurons and glia that make up the entire central nervous system (1). Postnatally, these NSCs persist only in discrete regions of the adult mammalian brain, namely, the neurogenic niches including the subventricular zone (SVZ) of the lateral ventricle and the subgranular zone (SGZ) of the hippocampus (2, 3). Neurons generated from the SVZ-NSCs migrate to the olfactory bulb and play a role in olfaction, whereas those from the SGZ remain in the dentate gyrus and participate in learning and memory (4, 5).

In contrast to region-restricted NSCs, the ubiquitously distributed resident glial cells are emerging as a cell source for generation of new neurons through fate reprogramming (6–9). Despite controversies (10–12), fate reprogramming can be accomplished under certain injury paradigms (13–16) or through controlling the expression of a single or a combination of fate-determining factors (17–27). Induction of new neurons from resident glia has been achieved in multiple nonneurogenic regions, such as the striatum, the cortex, the spinal cord, and the retina. Nevertheless, a functional neural network requires not only neurons, but also glia. Multilineage differentiation will be ideal to provide all three cell types for neural regeneration. Thus far, such multilineage reprogramming of resident glia remains to be determined.

In this study, we conducted a series of in vivo screens for new factors capable of reprogramming the fate of resident striatal astrocytes. We uncovered that a single transcription factor (TF), DLX2, is sufficient to reprogram resident astrocytes to become induced neural progenitor cells (iNPCs). Genetic lineage tracings validated the astrocyte origin and delineated the multiple fates of iNPCs. Single-cell RNA sequencing (scRNA-seq) further revealed that the DLX2-mediated reprogramming process resembles neurogenesis from NSCs.

Results

DLX2 Efficiently Initiates Neurogenesis in the Adult Mouse Striatum. We conducted a series of in vivo screens for factors that could induce neurogenesis in the adult mouse striatum. We focused on TFs specifying GABAergic neurons, which are the predominant subtype in the striatum. These factors were delivered into the striatum through lentivirus under the *bGFAP* promoter, which mainly targets astrocytes (18). New neurons were initially analyzed by staining for DCX, a marker that is transiently expressed in neuroblasts and immature neurons, but absent in the adult striatum (17, 18). These cells were imaged and quantified with a confocal microscope (*SI Appendix, Fig. S1*).

Significance

Outside the neurogenic niches, the adult brain lacks multipotent progenitor cells. In this study, we performed a series of in vivo screens and reveal that a single factor can induce resident brain astrocytes to become induced neural progenitor cells (iNPCs), which then generate neurons, astrocytes, and oligodendrocytes. Such a conclusion is supported by single-cell RNA sequencing and multiple lineage-tracing experiments. Our discovery of iNPCs is fundamentally important for regenerative medicine since neural injuries or degeneration often lead to loss/dysfunction of all three neural lineages. Our findings also provide insights into cell plasticity in the adult mammalian brain, which has largely lost the regenerative capacity.

Author contributions: Y. Zhang, B.L., G.C.H., and C.-L.Z. designed research; Y. Zhang, B.L., S.C., C.H., L.L.W., and Y. Zou performed research; Y.-X.F. contributed new reagents/analytic tools; Y. Zhang, B.L., G.C.H., and C.-L.Z. analyzed data; and Y. Zhang, B.L., G.C.H., and C.-L.Z. wrote the paper.

The authors declare no competing interest.

This article is a PNAS Direct Submission. A.K. is a guest editor invited by the Editorial Board.

Copyright © 2022 the Author(s). Published by PNAS. This article is distributed under [Creative Commons Attribution-NonCommercial-NoDerivatives License 4.0 \(CC BY-NC-ND\)](https://creativecommons.org/licenses/by-nc-nd/4.0/).

¹Y. Zhang and B.L. contributed equally to this work.

²To whom correspondence may be addressed. Email: Chun-Li.Zhang@utsouthwestern.edu or Gary.Hon@utsouthwestern.edu.

This article contains supporting information online at <http://www.pnas.org/lookup/suppl/doi:10.1073/pnas.2107339119/-/DCSupplemental>.

Published March 7, 2022.

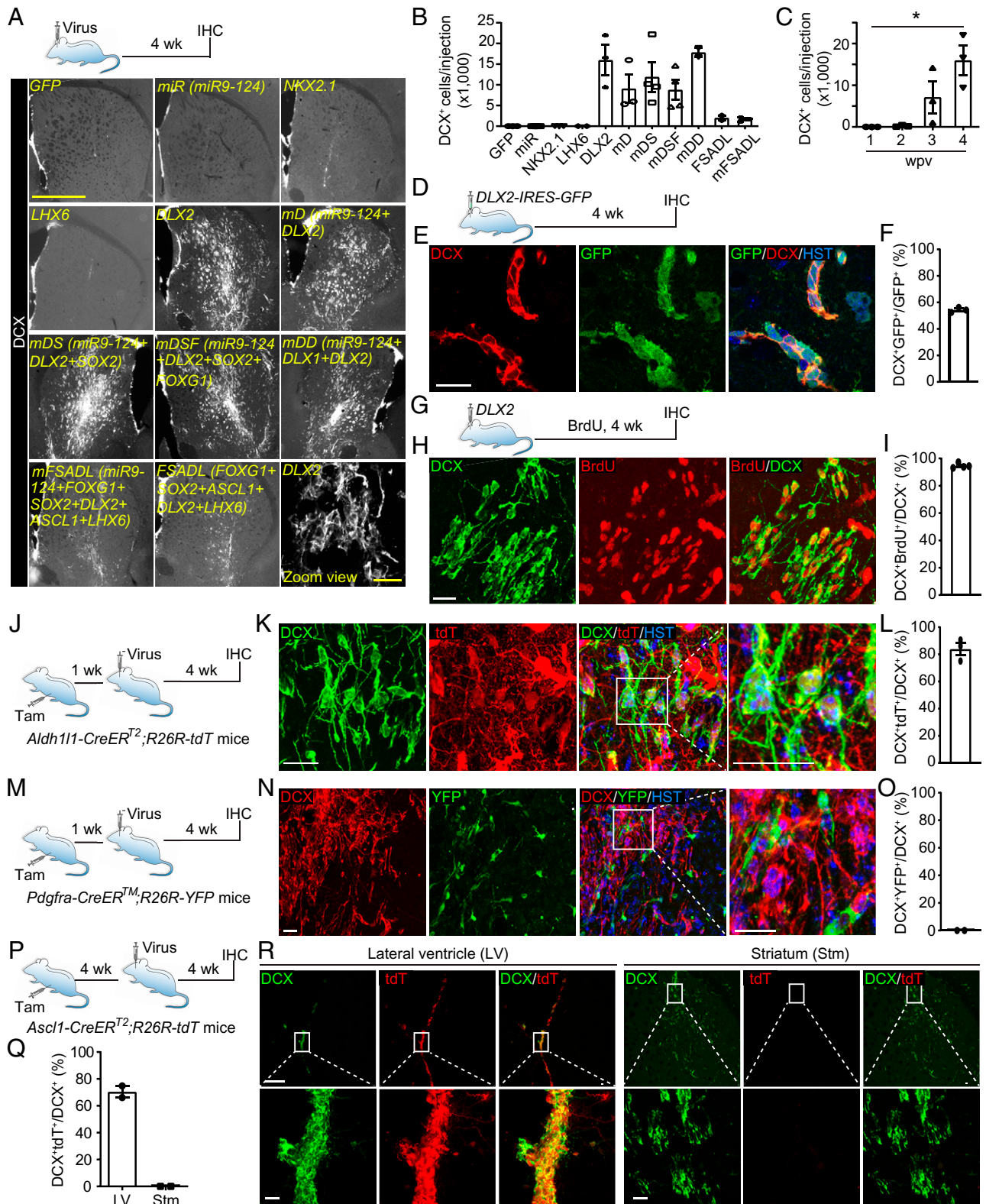


Fig. 1. DLX2 elicits neurogenesis from adult resident astrocytes. (A) Images of DCX expression in the adult striatum injected with viruses expressing the indicated genes. IHC, immunohistochemistry. (Scale bars: 1 mm for lower-magnification views and 20 μ m for zoom view.) (B) Quantifications of induced DCX⁺ cells ($n = 2$ to 4 mice per condition). (C) A time-course analysis of DLX2-induced DCX⁺ cells [$n = 3$; * $P = 0.0083$ and $F(3,8) = 8.101$ by one-way ANOVA]. (D) Study design to analyze reprogramming efficiency. (E) Confocal images showing coexpression of DCX and GFP. (Scale bar: 20 μ m.) (F) Quantification of DLX2-mediated reprogramming efficiency ($n = 2,448$ GFP⁺ cells from three mice). (G) Study design to examine cell proliferation with BrdU incorporation. (H) Confocal images showing BrdU-labeled DCX⁺ cells. (Scale bar: 20 μ m.) (I) Quantification of BrdU-labeled DCX⁺ cells ($n = 230$ DCX⁺ cells from four mice). (J) Study design to trace adult astrocytes and their derivatives. (K) Confocal images of astrocyte-derived DCX⁺ cells indicated by tdT. (Scale bars: 20 μ m.) (L) Quantification of astrocyte-derived DCX⁺ cells ($n = 421$ DCX⁺ cells from three mice). (M) Study design to trace NG2 glia and their derivatives. (N) Confocal images showing absence of the YFP reporter in DCX⁺ cells. (Scale bars: 20 μ m.) (O) DLX2-induced DCX⁺ cells do not come from NG2 glia ($n = 384$ DCX⁺ cells from two mice). (P) Study design to trace endogenous NSCs and their derivatives. (Q) DLX2-induced DCX⁺ cells do not come from endogenous NSCs ($n = 180$ DCX⁺ cells for LV and $n = 350$ DCX⁺ cells for Stm from two mice). LV, lateral ventricle; Stm, striatum. (R) Confocal images showing expression of DCX and the tdT reporter in the indicated brain regions. tdT⁺ cells are not present in the adult striatum. (Scale bars: 200 μ m for Upper and 20 μ m for Lower.).

When examined at 4 wk post virus injections (wpv), DCX⁺ cells were not detectable in the striatum injected with virus expressing miR9-124, NKX2.1, or LHX6 (Fig. 1 *A* and *B*). In contrast, the DLX2-containing groups all produced DCX⁺ cells. A time-course analysis of the DLX2-alone group showed that DCX⁺ cells were not detectable at 1 wpv, but greatly increased from 2 to 4 wpv [Fig. 1 *C*; $P = 0.0083$ and $F(3,8) = 8.101$ by one-way ANOVA].

The reprogramming efficiency was estimated by using the coexpressed GFP reporter in a virus expressing DLX2-IRES-GFP (Fig. 1 *D*). Unlike DLX2, which was quickly down-regulated after reprogramming, GFP was more stable and could still be detected at 4 wpv (*SI Appendix*, Fig. *S2*). About half (54.32%) of DLX2 virus-transduced GFP⁺ cells were transformed into DCX⁺ cells, suggesting a relatively high efficiency (Fig. 1 *E* and *F*). To determine whether these DCX⁺ cells were newly generated, we treated DLX2-injected mice with bromodeoxyuridine (BrdU)-containing drinking water for 4 wk (Fig. 1 *G*). In the noninjected contralateral side, BrdU⁺ cells were rarely observed, and they were mainly OLIG2⁺ oligodendrocyte precursor cells (OPCs) or IBA1⁺ microglia (*SI Appendix*, Fig. *S3A*). In contrast, many BrdU⁺DCX⁺ cells were detected in the DLX2 virus-injected side (Fig. 1 *H* and *I*), with the remaining BrdU⁺DCX⁻ cells being SOX9⁺ astrocytes, OLIG2⁺ OPCs, or IBA1⁺ microglia (*SI Appendix*, Fig. *S3B*). Together, these results indicate that DLX2 efficiently induced DCX⁺ cells, which passed through a proliferative state.

DLX2-Induced Neurogenesis Arises from Resident Astrocytes.

To confirm the cell origin for DLX2-induced DCX⁺ cells, we conducted lineage-tracing experiments. Astrocytes were traced in *Aldh1l1-CreER^{T2};R26R-tdTomato (tdT)* mice after three daily tamoxifen (Tam) treatments (*SI Appendix*, Fig. *S4A*). We found that 97.18% and 98.39% of tdT⁺ striatal cells were positive for the astrocyte markers ALDH1L1 and ALDOC, respectively (*SI Appendix*, Fig. *S4 B–D*). The remaining tdT⁺ cells were APC⁺ oligodendrocytes (2.54 ± 2.54%) and NeuN⁺ neurons (0.21 ± 0.21%). Such results indicate that striatal astrocytes can be efficiently traced in these mice, consistent with a previous report (28). These mice were then injected with DLX2 virus 1 wk post Tam (Fig. 1 *J*). DCX⁺ and tdT⁺ cells were imaged and quantified with confocal microscopy at 4 wpv (*SI Appendix*, Fig. *S5*). We found that 83.88% of DLX2-induced DCX⁺ cells were colabeled with tdT, indicating an origin of resident astrocytes (Fig. 1 *K* and *L*).

Since lentivirus under the *hGFAP* promoter also transduces a fraction of NG2 glia (18), we examined their contribution to DLX2-induced DCX⁺ cells by using the *Pdgfra-CreERTM;R26R-YFP* mice. In the control experiment, 80.16% of NG2 glia, but not NeuN⁺ neurons or ALDOC⁺ astrocytes, could be traced by the reporter YFP (*SI Appendix*, Fig. *S4 E–G*), showing cell-type specificity of this lineage-tracing mouse line. These mice were then injected with DLX2 virus and examined at 4 wpv (Fig. 1 *M*). Immunohistochemistry showed robust induction of DCX⁺ cells in the DLX2-injected striatum; however, none of them were YFP⁺, excluding NG2 glia as a cell origin for these DCX⁺ cells (Fig. 1 *N* and *O*).

Previous studies indicate that brain injury may lead to migration of endogenous neuroblasts in the SVZ to the lesion area (29). This raised a possibility that DLX2-induced DCX⁺ cells might just be the migrating endogenous neuroblasts. We examined this possibility in adult *Ascl1-CreER^{T2};R26R-tdT* mice (18, 30). These mice were treated with Tam and subsequently injected with virus (Fig. 1 *P*). When examined at 4 wpv,

~70.47% of DCX⁺ cells were labeled with tdT in the SVZ, whereas tdT⁺ neuroblasts/progenitors were not observed in the DLX2 virus-injected striatum (Fig. 1 *Q* and *R*), clearly excluding their contribution to DLX2-induced neurogenesis.

Collectively, these above multiple lineage-tracing results indicate that DLX2-induced DCX⁺ cells originate from resident astrocytes, but not from NG2 glia or SVZ neuroblasts/progenitors.

DLX2 Rapidly Reprograms Astrocytes into ASCL1⁺ iNPCs.

Next, we examined the DLX2-mediated reprogramming process by immunohistochemistry and genetic lineage tracing. During endogenous neurogenesis, ASCL1⁺ NPCs precede DCX⁺ cells (30). While not detected at 1 wpv, DLX2 induced thousands of ASCL1⁺ cells in the injection area at 2 or 3 wpv (Fig. 2 *A–C*). Genetic lineage tracing in Tam-treated *Aldh1l1-CreER^{T2};R26R-tdT* mice confirmed that DLX2-induced ASCL1⁺ cells originated from resident astrocytes (*SI Appendix*, Fig. *S6 A–C*). By 4 wpv, both the expression level and the number of ASCL1⁺ cells were reduced (Fig. 2 *B* and *C*). Such a time course of ASCL1 expression contrasted with that of DCX, which was first robustly detected at 3 wpv and further increased at 4 wpv (Fig. 1 *C*), suggesting that ASCL1⁺ NPCs gave rise to DCX⁺ cells. Indeed, we could find some transitional ASCL1⁺DCX⁺ cells at 3 wpv, and these cells were traced back to astrocytes indicating a lineage progression from astrocytes to ASCL1⁺ cells to DCX⁺ neuroblasts (*SI Appendix*, Fig. *S6 D* and *E*). To further validate such a cell-lineage progression, we employed the adult *Ascl1-CreER^{T2};R26R-tdT* mice. After injection of DLX2 virus, mice were treated with Tam for 1 wk starting at 2 wpv (Fig. 2 *D*). At 4 wpv, about 82.63% of DCX⁺ cells were genetically labeled with the reporter tdT, confirming an origin of the DLX2-induced ASCL1⁺ NPCs (Fig. 2 *E* and *F*). Of note, tdT⁺ cells were not observed in the control virus-injected striatum.

We next examined whether the DLX2-reprogrammed astrocytes lost their astrocyte identity. The adult *Aldh1l1-CreER^{T2};R26R-tdT* mice were first injected with DLX2 virus and then treated with Tam starting at 2 wpv for 5 d (Fig. 2 *G*). When examined at 4 wpv, we observed that 92.70% of DCX⁺ cells were not labeled by tdT (Fig. 2 *H* and *I*), indicating that DLX2 has rapidly reprogrammed the fate of resident astrocytes. The remaining 7.3% of DCX⁺tdT⁺ cells were likely derived from those astrocytes still undergoing fate conversion at 2 wpv. Together, these above results show that DLX2-reprogrammed resident astrocytes rapidly lose their astrocyte identity and become iNPCs that further give rise to DCX⁺ neuroblasts (Fig. 2 *J*).

iNPCs Generate CTIP2⁺ GABAergic Neurons.

To determine whether iNPCs gave rise to mature neurons, we traced them in *Ascl1-CreER^{T2};R26R-tdT* mice after virus injections and Tam treatments (*SI Appendix*, Fig. *S7A*). DLX2 alone was able to generate about 2,000 tdT-traced NeuN⁺ neurons when examined at 8 wpv (*SI Appendix*, Fig. *S7 B* and *C*). We also examined whether DLX2 activity could be promoted by neurotrophic factors, including BDNF, NOG, and the NT3 mutant p75-2, all of which were shown to promote neuronal maturation (17, 18, 22, 31). Lentiviruses encoding these factors were coinjected with DLX2 virus and examined at 8 wpv in *Ascl1-CreER^{T2};R26R-tdT* mice. BDNF slightly increased, whereas BDNF-NOG or p75-2 decreased, the number of DLX2-induced NeuN⁺tdT⁺ cells (*SI Appendix*, Fig. *S7 B* and *C*). Of note, NeuN⁺tdT⁺ cells were not observed in the control BDNF-NOG alone condition. New neurons were confirmed by BrdU labeling, with abundant BrdU⁺NeuN⁺ cells in

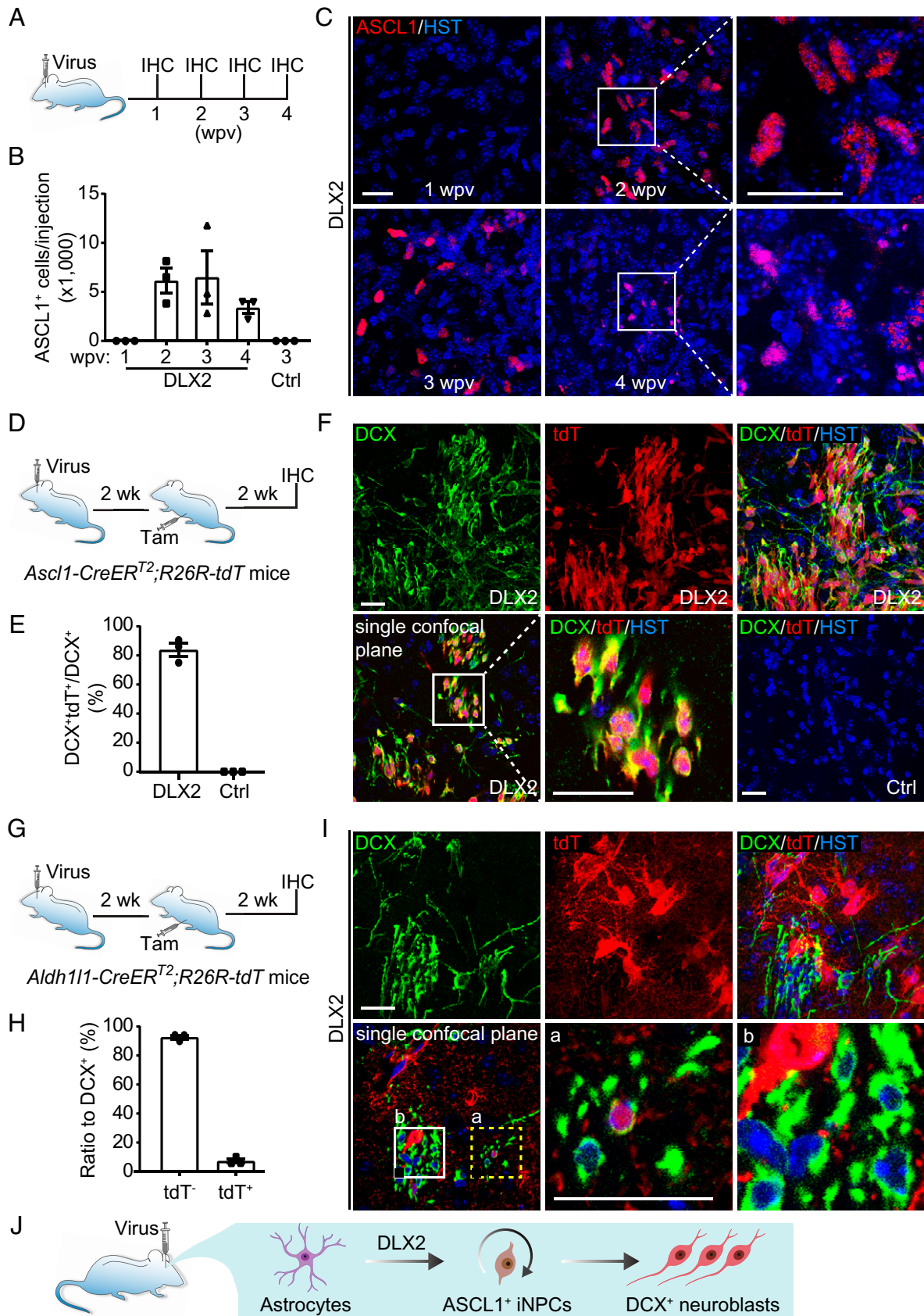


Fig. 2. Reprogrammed astrocytes become ASCL1⁺ NPCs. (A) Study design to analyze DLX2-induced ASCL1⁺ cells. (B) A time-course analysis of DLX2-induced ASCL1⁺ cells ($n = 3$ mice per time point). (C) Confocal images of DLX2-induced ASCL1⁺ cells at the indicated time points. (Scale bars: 20 μm .) (D) Study design to trace DLX2-induced ASCL1⁺ cells and their derivatives. (E) Quantification of DLX2-induced DCX⁺ cells transiting through an ASCL1⁺ stage ($n = 365$ DCX⁺ cells from three mice). (F) Confocal images of ASCL1-derived DCX⁺ cells indicated by tdT. tdT⁺ or DCX⁺ cells were not detected in the control (Ctrl) virus-injected striatum. (Scale bars: 20 μm .) (G) Study design to analyze the timing of astrocyte reprogramming. (H) Quick loss of astrocyte identity when reprogrammed by DLX2. Quantification was conducted at 4 wpv ($n = 463$ DCX⁺ cells from three mice). (I) Confocal images of lineage-traced cells showing a quick loss of astrocyte identity when reprogrammed. Enlarged views of the boxed regions are shown in *Right*. (Scale bars: 20 μm .) (J) A schematic summary of the reprogramming process.

the DLX2–BDNF group, but not in the control BDNF-alone group (*SI Appendix, Fig. S8*).

Neuronal subtypes were then examined at 12 wpv in adult *Ascl1-CreER^{T2};R26R-tdT* mice (Fig. 3*A*), a time point at which the induced NeuN⁺tdT⁺ neurons acquired complex morphology (Fig. 3*B*). Approximately 88.69% of induced neurons were GABAergic, while CHAT⁺ or VGLUT2⁺ neurons were not detected (Fig. 3*C* and *D*). Interestingly, CTIP2 (also known as BCL11B), a TF critical for striatal development and specification of medium spiny neurons (32), was observed in 51.00% of NeuN⁺tdT⁺ neurons (Fig. 3*C*, *E*, and *G*). Since an examination of the early reprogramming process showed that CTIP2 was not directly induced by ectopic DLX2 (*SI Appendix, Fig. S9*), its expression in NeuN⁺tdT⁺ cells rather suggests that these cells gained a striatal identity. Nonetheless, the number of DARPP32⁺ cells was low, indicating that a majority of these induced CTIP2⁺ neurons were not developed into mature medium spiny neurons at this stage. CALB2 (also known as calretinin) was observed in both NeuN⁺- and NeuN⁻-induced neurons (Fig. 3*F*); the latter was also previously detected in the normal mouse forebrain and may represent a new class of calretinin-positive neurons (33). On the other hand, PVALB, SST, or CALB1 was not detected in these NeuN⁺tdT⁺ neurons (Fig. 3*C*).

iNPCs Are Multipotent. In addition to neuroblasts and neurons, we also noticed that DLX2 induced glia-like cells in the striatum. An estimate showed a significantly increased number of SOX9⁺ astrocytes surrounding the DLX2-injected regions [*SI Appendix, Fig. S10*; $P = 0.0021$ and $F(2,6) = 20.34$ by one-way ANOVA]. We then surveyed both neurons and glial cells induced by DLX2 through a time-course analysis in adult *Ascl1-CreER^{T2};R26R-tdT* mice (Fig. 4*A*). At 4 wpv, DCX⁺ and NeuN⁺ cells represented about 73.41% and 4.45% of DLX2-induced tdT⁺ cells, respectively (Fig. 4*B*). The ratio of glial cells, indicated by OLIG2, ALDH1L1, or ALDOC, was about 12% (Fig. 4*B*). SOX10⁺OLIG2⁺tdT⁺ OPCs were detected at this time point (*SI Appendix, Fig. S11 A and B*). By 8 wpv, more neuroblasts differentiated into neurons, leading to a decrease of DCX⁺ cells (62.63%) and a corresponding increase of NeuN⁺ cells (22.00%), whereas the ratios of OLIG2⁺ glia (12%) and ALDH1L1⁺ or ALDOC⁺ astrocytes (12%) remained unchanged (Fig. 4*C*). After another 4 wk, DCX⁺ cells decreased to 10.15%, while the ratio of neurons remained constant (Fig. 4*D* and *E*). In contrast, more APC⁺tdT⁺ oligodendrocytes appeared, and the fraction of ALDH1L1⁺tdT⁺ or ALDOC⁺tdT⁺ astrocytes increased to 36% (Fig. 4*D* and *E*). Interestingly, both SOX10⁺OLIG2⁺tdT⁺ OPCs and MBP⁺OLIG2⁺tdT⁺ oligodendrocytes could be observed at this later time (*SI Appendix, Fig. S11 C*). Thus, for the first 8 wk, the ratio of neurogenesis to gliogenesis was 4:1, with 80% of DLX2-induced tdT⁺ cells as neuroblasts/neurons and the remaining 20% as glial cells. By 12 wpv, the glia fraction greatly increased, with astrocytes and oligodendrocytes representing about half of the total DLX2-induced tdT⁺ cells (Fig. 4*D*). Two mechanisms might account for the increased number of glial cells at later time points. On one hand, glial cells might proliferate in response to a regeneration niche; however, they morphologically resembled protoplasmic astrocytes (Fig. 4*F*), and none of them were Ki67⁺, a marker of proliferating cells (Fig. 4*G*). On the other hand, iNPCs might proliferate and be more prone to differentiate into glial cells. We indeed observed that 2% of all tdT⁺ cells were Ki67⁺ cells (Fig. 4*F* and *G*). They morphologically resembled ASCL1⁺ or OLIG2⁺ cells,

both of which might give rise to oligodendrocytes and astrocytes. Thus, iNPCs reprogrammed from astrocytes largely sequentially generate neurons and glial cells (Fig. 4*H*).

scRNA-Seq Captures the DLX2-Mediated Reprogramming Trajectory. To define the reprogramming process, we performed scRNA-seq of tdT⁺ cells that were sorted from Tam-treated and virus-injected *Aldh111-CreER^{T2};R26R-tdT* mice at 4 wpv (*SI Appendix, Figs. S12 and S13A*). Two samples were prepared: *Lenti-DLX2* ($n = 5$ mice) and *Lenti-GFP* ($n = 4$ mice). After data-quality filtering, this dataset consisted of 5,756 cells from the *Lenti-DLX2* group and 4,610 cells from the *Lenti-GFP* control. We then performed batch correction (34), clustering, and dimensionality reduction (35)—all standard bioinformatic methods used to analyze scRNA-seq data—to generate a map of all analyzed cells (Fig. 5*A*). In this map, each cluster of cells represented by the same color suggests that these cells share transcriptome-wide similarity and thereby likely represents a distinct cell state, cell type, or subtype. We then used a panel of known marker genes to assign broad cell-type identity to each cell cluster (Fig. 5*B* and *SI Appendix, Fig. S13B*). Specifically, we identified expected cell types in the brain, such as neural cells (astrocytes, NPCs, neuroblasts, NG2 glia, and oligodendrocytes), immune cells (T cells, B cells, myeloid cells, macrophages, and microglia), and endothelial cells. Immunohistochemistry confirmed that these nonneural cells could indeed be traced in virus-injected regions of Tam-pretreated *Aldh111-CreER^{T2};R26R-tdT* mice (*SI Appendix, Fig. S14*).

To focus on cells with the most relevance to DLX2-mediated reprogramming, we selected neural clusters with enrichment for *Lenti-DLX2* cells (Fig. 5*C* and *SI Appendix, Fig. S13C*). Among these cells, 22.5% are unperturbed astrocytes, 15.2% are lenti-astrocytes, 12.9% are NPCs, 49.2% are neuroblasts, and 0.2% are neurons (*SI Appendix, Fig. S13D*). Pseudotime analysis [diffusion pseudotime, a commonly used pseudotime method (36)] identified a trajectory of transcriptional states during DLX2-mediated reprogramming across four broad neural cell clusters, in the order of astrocytes, lenti-astrocytes, NPCs, and neuroblasts (Fig. 5*C–E*). Pseudotime assumes and reflects the gradual change of the transcriptome and therefore suggests, but does not prove, the sequential order of cell-state progression during DLX2-induced reprogramming. This putative reprogramming trajectory is supported by several lines of evidence. First, cells from the *Lenti-DLX2* group expressed the astrocyte-lineage reporter *tdT* throughout the pseudotime trajectory (Fig. 5*D, Top*), consistent with our lineage-tracing results (Fig. 1*J–L*). Second, NPCs and neuroblasts from the *Lenti-DLX2* group expressed the lentiviral transgene (Fig. 5*D, Middle*). Interestingly, lentiviral expression decreased as reprogramming progressed, consistent with our immunohistochemistry result (*SI Appendix, Fig. S2B*). This is potentially due to epigenetic silencing of the *GFAP* promoter as cells exit astrocyte fate (*SI Appendix, Fig. S13E*). Third, this putative trajectory was enriched for cells from the *Lenti-DLX2* group (Fig. 5*D, Bottom*), consistent with our data that neuroblasts were specifically induced by DLX2, but not lentiviral transduction per se (Fig. 1*A* and *B*). Together, scRNA-seq shows that *Lenti-DLX2* astrocytes undergo cell-state changes toward neuroblasts (*Dcx* and *Calb2*) through a proliferating NPC intermediate, which is marked by the expression of *Cdk1*, *Mki67*, and *Ascl1* (*SI Appendix, Fig. S13 F–J*). Consistent with the lineage-tracing results (Fig. 4), generation of oligodendrocytes from reprogrammed cells is predicted from the activation of genes essential for their development in iNPCs, such as *Olig1* and *Olig2* (*SI Appendix, Fig. S13 K and L*).

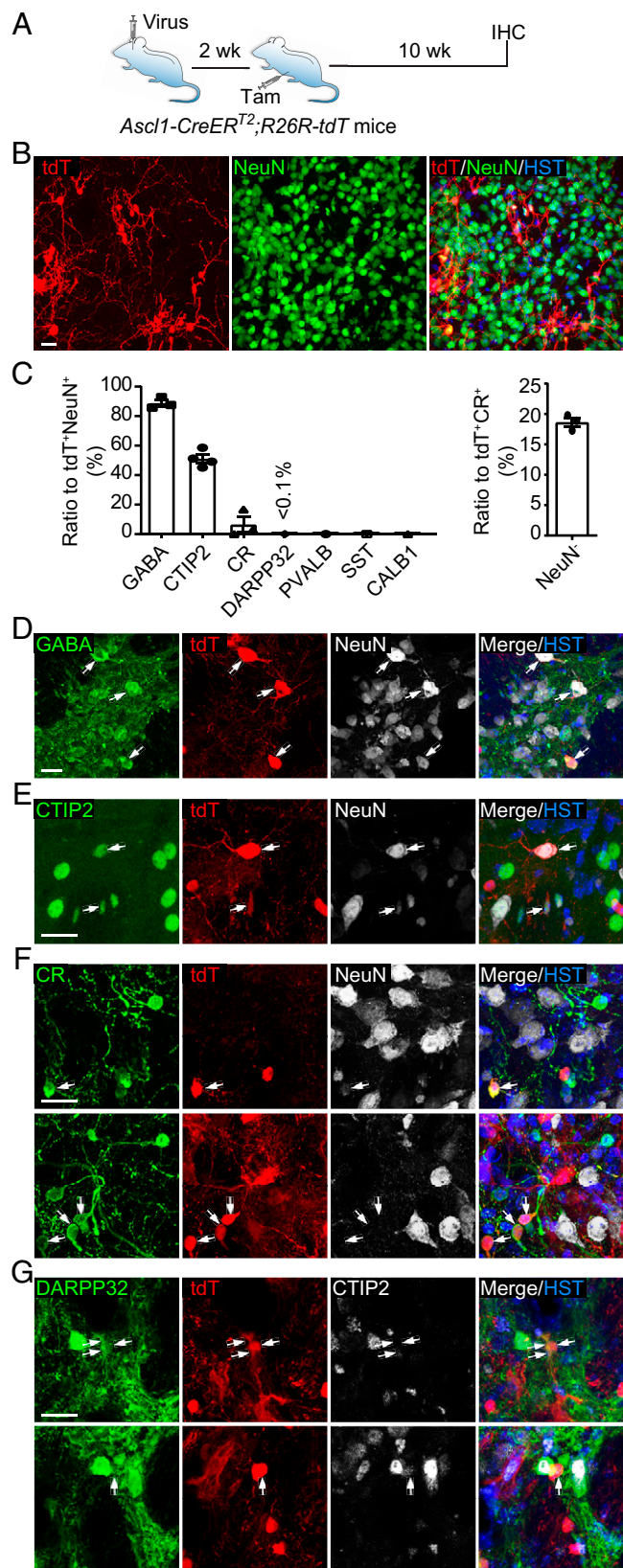


Fig. 3. Reprogrammed astrocytes generate mature neurons. (A) Study design to analyze DLX2-induced neurons. (B) Confocal images of DLX2-induced neurons with complex morphology at 12 wpv. (Scale bar: 20 μ m.) (C) Quantification of neuronal subtypes ($n = 3$ or 4 mice; $n = 451$ NeuN⁺tdT⁺ cells for GABA⁺NeuN⁺tdT⁺, CTIP2⁺NeuN⁺tdT⁺, and CR⁺NeuN⁺tdT⁺; $n = 6$ brain slices for each of the other markers; $n = 594$ tdT⁺ cells for CR⁺NeuN⁻tdT⁺ cells). (D) Confocal images showing DLX2-induced GABAergic neurons. (Scale bar: 20 μ m.) (E) Confocal images showing DLX2-induced CTIP2⁺ neurons. (Scale bar: 20 μ m.) (F) Confocal images showing DLX2-

Gene Regulatory Networks Underlying DLX2-Mediated Reprogramming. To identify gene programs dynamically regulated during DLX2-induced reprogramming, we conducted unsupervised clustering of genes to identify 12 expression patterns spanning 2,584 variably expressed genes among the *Lenti-DLX2* cells (Fig. 5F and Dataset S1). We reasoned that these genes are the most interesting because high variability of gene expression suggests dynamic regulation during reprogramming. These 12 expression patterns further fell into five broad patterns based on the timing of expression along pseudotime: astrocyte genes (clusters 6 and 0), lenti-astrocyte genes (clusters 2 and 10), transition genes (cluster 3), NPC genes (clusters 9, 7 and 1), and neurogenesis genes (clusters 4, 8, 5, and 11) (Fig. 5F). Consistently, known gene markers for astrocytes (*Id3*, *Aldh1l1*, and *Clu*), NPCs (*Ascl1*), cell cycle (*Cdk1*, *Ccna2*, and *Mki67*), and neurogenesis (*Dlx1*, *Dlx2*, *Dcx*, *Dlx6os1*, and *Calb2*) were assigned to their expected expression patterns. Notably, gene cluster 5 (neurogenesis genes) showed significant enrichment of putative targets of *Dlx1/2* in the developing mouse brain (37) ($P = 7.37e-35$, χ^2 test; SI Appendix, Fig. S13M), suggesting that DLX2 drives a similar regulatory program during reprogramming of astrocyte as in neural development.

To understand the functional relevance of these gene clusters, we performed Gene Ontology (GO) enrichment analysis for each cluster (Fig. 5F, GO terms, and Dataset S2). First, astrocyte genes (clusters 6 and 0) showed enrichment for metabolic terms like lipid metabolic process and glycogen metabolic process, suggesting a metabolic shift during astrocyte conversion. Second, lenti-astrocyte genes (clusters 2 and 10) were enriched for immune responses (cluster 10), likely a response to lentiviral infection. In addition, lipid metabolism-related terms were again enriched (cluster 2), the expression of which would later be silenced based on the expression pattern of cluster 2, further pointing to a metabolic shift. Third, transition genes (cluster 3) exhibited enrichment for terms related to metabolism in mitochondria, including mitochondrial translation, mitochondrial respiratory chain complex I assembly, and electron transport (Dataset S2). Since neurons, but not astrocytes, use oxidative phosphorylation as their main energy source (38), these data suggest that DLX2-transduced cells use cluster 3 genes to prepare their mitochondria for a switch to oxidative phosphorylation. Fourth, the NPC-enriched genes (clusters 9, 7, and 1) were dominated by those involved in the cell cycle. Cluster 9 genes were involved in the G1/S phase (DNA replication, DNA repair, etc.), while cluster 7 genes represented the G2/M phase (cell division, mitotic cytokinesis, etc.). In addition to cell-cycle-related terms, cluster 1 was also enriched for RNA-processing terms, suggesting that cells used cluster 1 genes to cope with the increased need for RNA synthesis during active cell cycles. Lastly, neurogenesis genes (clusters 4, 8, 5, and 1) were enriched in terms related to neural development, which notably included *Dcx*, *Dlx1/2*, *Dlx6os1*, and *Calb2* (cluster 5). Together, these results suggest that distinct gene regulatory programs, such as neurogenesis, metabolism, and immune responses, are coordinately regulated during DLX2-mediated reprogramming.

Finally, we used coexpression and regulatory relationships to construct gene regulatory networks (pySCENIC) (39) underlying DLX2-mediated reprogramming. We identified 430 regulons, each representing one TF and its putative target genes. We observed distinct patterns of regulon activity (derived from

induced CR⁺ neurons. (F, Upper) NeuN⁺CR⁺ neurons. (F, Lower) NeuN⁻CR⁺ neurons. (Scale bar: 20 μ m.) (G) Confocal images showing DLX2-induced striatal-like neurons. (G, Upper) DARPP32⁺CTIP2⁻ neurons. (G, Lower) DARPP32⁻CTIP2⁺ neurons. (Scale bar: 20 μ m.).

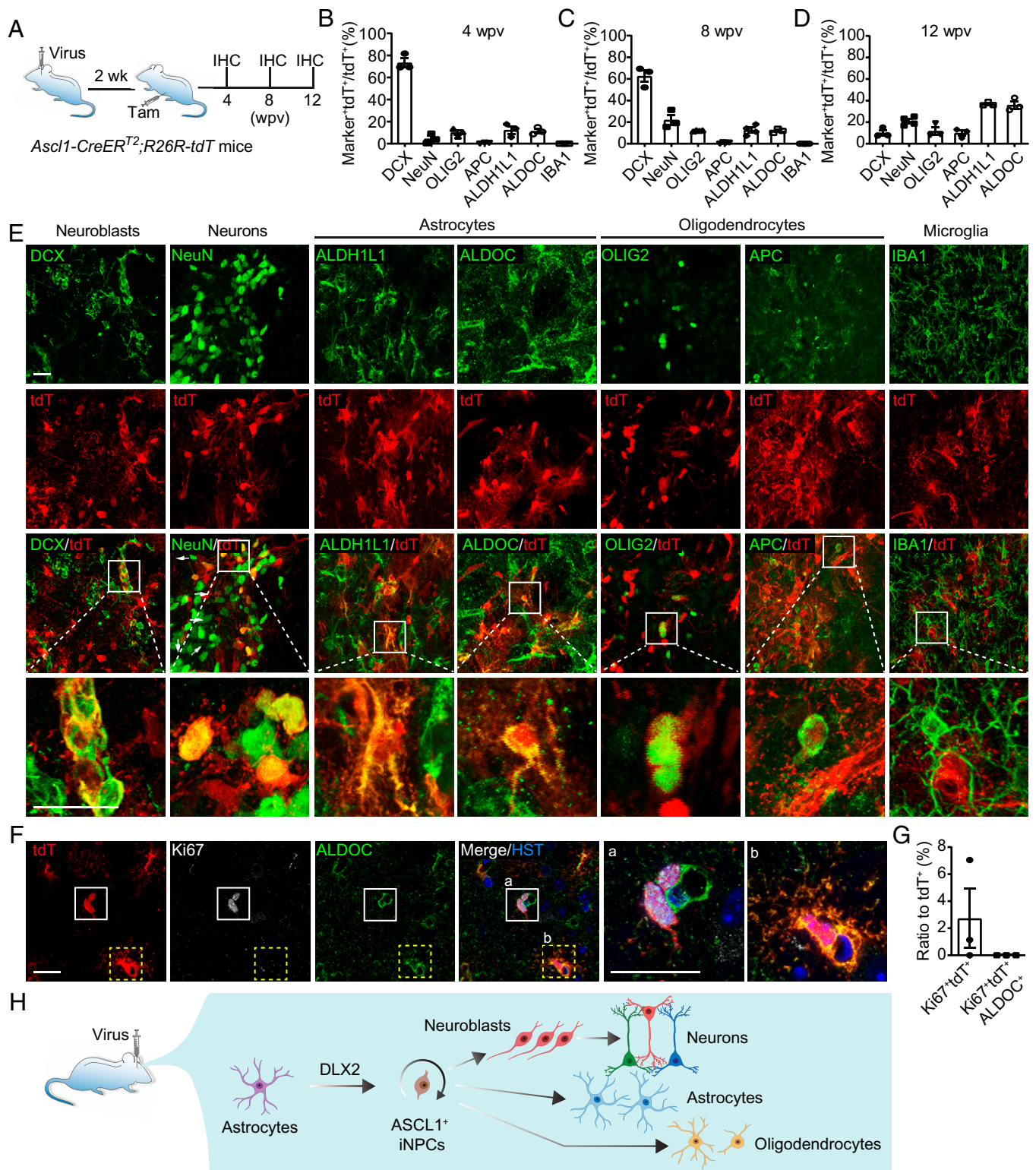


Fig. 4. Astrocyte-converted ASCL1⁺ cells are multipotent NPCs. (A) Study design for fate analysis of DLX2-induced ASCL1⁺ iNPCs. (B–D) Quantification of cell types derived from iNPCs at the indicated time points ($n = 5,487$ tdT⁺ cells from three mice for 4 wpv, $n = 7,982$ tdT⁺ cells from three or four mice for 8 wpv, and $n = 3,665$ tdT⁺ cells from three or four mice for 12 wpv). (E) Confocal images of multiple cell types derived from DLX2-induced ASCL1⁺ iNPCs at 12 wpv. (Scale bars: 20 μ m.) (F) Confocal images of proliferating iNPCs at 12 wpv. a, an enlarged view of proliferating iNPCs in the boxed region a; b, an enlarged view of iNPC-derived, nonproliferative astrocyte in the boxed region b. (Scale bars: 20 μ m.) (G) Quantification of proliferating iNPCs at 12 wpv ($n = 309$ tdT⁺ cells from three mice). (H) A schematic summary of the reprogramming process and cell identities.

expression levels of component genes) along the reprogramming trajectory (Fig. 5G). High activity score suggests activation and low activity score suggest repression of the regulon. For example, known neuronal regulators, including *Arx*, *Dlx1*,

Dlx5, and *Klf7*, are specifically active in neuroblasts. Consistent with published data, the *Dlx1* regulon was significantly enriched in putative *Dlx1/2* targets derived from perturbation and chromatin immunoprecipitation sequencing (37) (*SI*

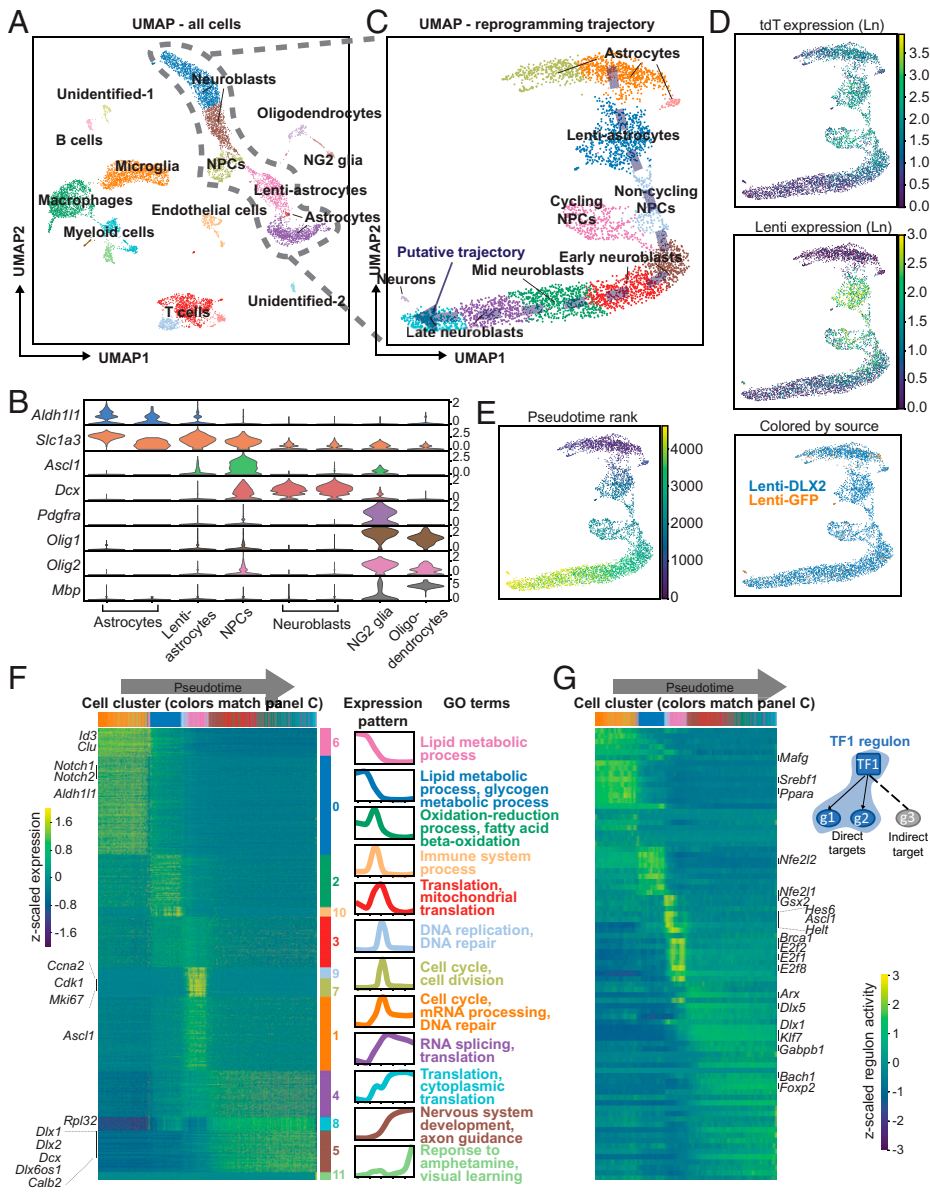


Fig. 5. Gene programs and regulatory networks underlying DLX2-induced reprogramming of adult astrocytes. (A) *Lenti-DLX2* and *Lenti-GFP* control cells are clustered. A total of 18 neural and nonneural cell types are identified by examining the expression of known marker genes, and two clusters could not be identified by these genes. A putative reprogramming trajectory (gray dashed box) consisting of astrocytes, lenti-astrocytes, NPCs, and neuroblasts is further examined in C. (B) A panel of marker genes are used to identify astrocytes, NPCs, neuroblast, NG2 glia, and oligodendrocytes. A more comprehensive panel can be found in *SI Appendix*, Fig. S13B. (C) Sub-clustering of the putative reprogramming trajectory from astrocytes to lenti-astrocytes, NPCs, and neuroblasts reveals heterogeneity within each cell type. Putative reprogramming trajectory is indicated by the dark purple arrow. (D) Astrocyte lineage tracer *tdT* (Top) and lentiviral transcript (Middle) are expressed along the reprogramming trajectory. The trajectory consists of mainly *Lenti-DLX2*, along with a few *Lenti-GFP* cells (D, Bottom). (E) Diffusion pseudotime is calculated. Cells are then ranked based on their pseudotime (low rank = early pseudotime). (F) Unsupervised clustering identifies 12 clusters of 2,584 highly variable genes showing five major expression patterns along pseudotime: astrocyte genes (clusters 6 and 0), lenti-astrocyte genes (clusters 2 and 10), transition genes (cluster 3), NPC genes (clusters 9, 7, and 1), and neurogenesis genes (clusters 4, 8, 5, and 11). GO terms enriched in each gene cluster highlight the associated biological processes. (G) Gene regulatory network analysis identifies potential regulators of each stage of reprogramming. For a list of all regulons shown here, see *Dataset S4*. UMAP, Uniform Manifold Approximation and Projection.

Appendix, Fig. S13 N and O). *Helt*, a TF required for development of GABAergic neurons (40), was active in noncycling NPCs. *Ascl1* was similarly active in noncycling NPCs (30). In addition, known regulators of the cell cycle (e.g., *E2f1*) and DNA repair (e.g., *Brca1*) were specifically active in NPCs. Supporting the notion that reprogrammed astrocytes shift their metabolism from lipid metabolism to oxidative phosphorylation from the gene-clustering analysis, two lipid metabolism regulators, *Srebf1* and *Ppara* (41, 42), showed specific activity in astrocytes that decreases during reprogramming. Finally, some regulon-governing TFs potentially work synergistically. For example, small MAF proteins, including MAFG, have been shown to dimerize with CNC protein family members, such as NRF1, NRF2 (whose precursors are NFE2L1 and NFE2L2, respectively), and BACH1 (43). *Mafg*, *Nfe2l1*, and *Nfe2l2* regulons were identified as lenti-astrocyte-specific, suggesting that their interaction may play a role in reprogramming.

Neurogenic Reprogramming of Resident Astrocytes by DLX2-Induced Regulons. To examine a potential role of these identified regulons, we focused on the DLX family since DLX2 induced not only its endogenous counterpart, but also *Dlx1*

and *Dlx5* (Fig. 5G). Interestingly, DLX2, DLX1, and DLX5 share binding properties in ganglionic eminences (37). As a negative control, we also included DLX6, which is primarily expressed in differentiated cells (44). Lentiviruses encoding these factors were then individually delivered into the striatum (*SI Appendix*, Fig. S15A). When analyzed at 4 wpv, DLX5 induced more than 10,000 DCX⁺ cells surrounding the injected region, comparable to that induced by DLX2 (*SI Appendix*, Fig. S15B). DLX1 also induced many DCX⁺ cells, albeit to a lesser degree. In contrast, no DCX⁺ cells were observed in DLX6-injected brains (*SI Appendix*, Fig. S15 B and C). To confirm the astrocyte origin, we employed the Tam-treated *Aldh1l1-CreER^{T2};R26R-tdT* mice (*SI Appendix*, Fig. S15D). We found that 88.73% of DCX⁺ cells induced by DLX1 or DLX5 could be genetically labeled by tdT, indicating an origin of resident astrocytes (*SI Appendix*, Fig. S15 E and F). Cell-proliferation assays further showed that 89.71 to 92.15% of these DLX1- or DLX5-induced DCX⁺ cells incorporated BrdU (*SI Appendix*, Fig. S15 G–I), suggesting that they passed through a proliferative progenitor state. To determine whether endogenous *Dlx1* and/or *Dlx5* were also required for the reprogramming activity of ectopic DLX2, we knocked down

their expression through short hairpin RNAs (*SI Appendix, Fig. S16A*). Nonetheless, down-regulation of either *Dlx1*, *Dlx5*, or their combination failed to significantly change the number of DLX2-induced DCX⁺ cells (*SI Appendix, Fig. S16 B–D*), suggesting that DLX2, DLX1, and DLX5 may play redundant roles during reprogramming.

DLX2-Mediated Reprogramming Requires Suppression of Notch Signaling. In addition to the DLX family regulons, we also examined Notch signaling since it is highly active in astrocytes, and its down-regulation is sufficient to initiate a neurogenic program (13–15). Consistently, both *Notch1* and *Notch2* were detected in cluster 0 astrocytes, but not in other cell clusters, during DLX2-mediated reprogramming (Fig. 5*F* and *Dataset S1*). We used the cleaved Notch1 intracellular domain (NICD) to assess the role of Notch signaling. Adult mice were intracerebrally injected with a mixture of DLX2 virus and a virus expressing GFP (as a control) or NICD under the *hGFAP* promoter (*SI Appendix, Fig. S17A*). Confirming previous results, DCX⁺ cells could be abundantly detected in the striatum injected with DLX2 and GFP viruses (*SI Appendix, Fig. S17 B and C*). In contrast, coexpression of NICD with DLX2 significantly reduced the number of DCX⁺ cells (*SI Appendix, Fig. S17 B and C*; $P = 0.0286$ by two-tailed t test), indicating that suppression of Notch signaling is required for DLX2 to induce reprogramming. To determine whether DLX2-mediated reprogramming is cell-autonomous, we analyzed expression of DLX2 and the induced ASCL1 at 2 wpv (*SI Appendix, Fig. S17D*). DLX2 was detectable in ~80% of ASCL1⁺ cells (*SI Appendix, Fig. S17 E and F*), suggesting that DLX2 cell-autonomously induced ASCL1 expression and initiated subsequent cell-fate reprogramming. Such a result is consistent with the notion that DLXs promote proneural programs through repressing Notch signaling (37).

The DLX2-Mediated Reprogramming Process Resembles Endogenous Neurogenesis. Like endogenous neurogenesis, DLX2-induced reprogramming transitions through an NPC state. Thus, we next asked if these two processes also resemble each other transcriptionally. To this end, we integrated publicly available scRNA-seq maps from wild-type (WT) embryonic day 18.5 (E18.5) mouse brains (cortex, hippocampus, and SVZ) (GEO dataset [GSE93421](#)) for comparisons between DLX2-induced and endogenous neurogenesis. After data-quality filtering, this dataset consisted of 5,756 cells from the *Lenti-DLX2* group, 4,611 cells from the *Lenti-GFP* control, and 19,964 cells from the WT E18.5 brains. Single cells from reprogramming and WT E18.5 datasets have comparable numbers of transcripts and genes detected per cell (*SI Appendix, Fig. S18A*). After batch correction, clustering, dimensionality reduction, and cell-type annotation, we similarly chose to focus on astrocytes, lenti-astrocytes, NPCs, and neuroblasts that together form the main reprogramming/neurogenesis trajectory (Fig. 6*A and B* and *SI Appendix, Fig. S18 B and C*).

We compared the gene-expression programs in DLX2-induced and endogenous neurogenesis based on pseudotime (Fig. 6*B* and *SI Appendix, Fig. S18D*). Four groups of genes were previously identified to be sequentially regulated during adult neurogenesis in the mouse SVZ (45). They are involved in NSC quiescence, activation, cell cycle, and neurogenesis. We observed striking parallels in the activation states of these gene sets between DLX2-induced and endogenous embryonic neurogenesis (Fig. 6*C*). We also examined two cohorts of genes defining NSC quiescence and activation during adult hippocampal neurogenesis (46) and found that they were similarly dynamically

regulated with the progression of DLX2-mediated astrocyte reprogramming (*SI Appendix, Fig. S18E*). Such analyses of stereotypical marker genes clearly show that DLX2-induced astrocytes activate molecular processes typically found in endogenous quiescent NSCs (qNSCs). Interestingly, the repression of quiescence genes (*Id3* and *Clu*) and induction of activation genes (*Rpl32*) occurs abruptly in reprogramming, in contrast to the gradual changes observed in E18.5 neurogenesis (Fig. 6*C*). These results suggest that DLX2-induced neurogenesis starts from a stable quiescent cell state.

To identify differences between induced and endogenous neurogenesis, we performed differential gene-expression analysis between cells from the DLX2 group and WT E18.5 brain cells (*Dataset S3*). We observed that the number of differentially expressed genes was highest in the first half of the trajectory (up until mid NPCs) and dropped dramatically as cells entered the neuroblast state (Fig. 6*D, Left*). This indicates that induced and endogenous neurogenesis transcriptionally differ in the early stage, but converge toward neurogenesis. This difference in the early stage is also reflected by the segregation between astrocytes from reprogramming and astrocytes/qNSCs from E18.5 datasets (Fig. 6*A and B*). Two examples of difference were noteworthy. First, cells undergoing endogenous neurogenesis expressed cell-cycle genes earlier in pseudotime (states 1 to 3, NSCs/astrocytes) when compared to cells undergoing DLX2-induced neurogenesis (states 4 to 6, NPCs) (Fig. 6*D, Center*). This was in accordance with our observation above that reprogrammed astrocytes went through a molecular transition resembling activation of qNSCs, whereas WT E18.5 brain cells started from an activated NSC state. Second, early in pseudotime, cells undergoing induced neurogenesis activated the expression of viral defense genes (Fig. 6*D, Right*), consistent with our previous observation (Fig. 5*F*, cluster 10). Interestingly, this immune response declined toward the NPC state. Taken together, differential expression analysis reveals that the difference between induced and endogenous neurogenesis is in part due to cell-cycle activation and early responses to viral transduction in reprogrammed cells.

Given the observed differences, we reasoned that DLX2-induced reprogramming in adult mice might resemble adult neurogenesis more than embryonic neurogenesis, since adult neurogenesis similarly starts from a quiescent cell state. To test this, we integrated our reprogramming dataset with an scRNA-seq dataset of adult neurogenesis in the hippocampus (GSE104323) (47). Only cells from postnatal day 18 (P18), P19, P23, P120, and P132 mice in the adult neurogenesis dataset were used for analysis. After data-quality filtering, batch correction, clustering, dimensionality reduction, and selecting only relevant cell types that comprise the main trajectory, this dataset consisted of 4,039 cells from the *Lenti-DLX2* group, 182 cells from the *Lenti-GFP* control (because the reprogramming trajectory is depleted of control group cells), and 3,250 cells from the adult hippocampus (*SI Appendix, Fig. S19A*). Despite differences in platform and processing pipelines, we observed that adult neurogenesis aligns well with DLX2-induced reprogramming. Notably, astrocytes from the two datasets cocluster (*SI Appendix, Fig. S19B*), suggesting that the starting cell states are similar. After calculating diffusion pseudotime (*SI Appendix, Fig. S19C*), we similarly examined established neurogenesis genes in adult neurogenesis cells (*SI Appendix, Fig. S19 D and E*). All examined genes followed the expected expression patterns and resembled DLX2-induced reprogramming more than E18.5 neurogenesis. For example, quiescence and activation genes also show an abrupt change (*Id3*, *Clu*, and *Rpl32* in *SI Appendix, Fig. S19D*; all genes in *SI Appendix, Fig. S19E*).

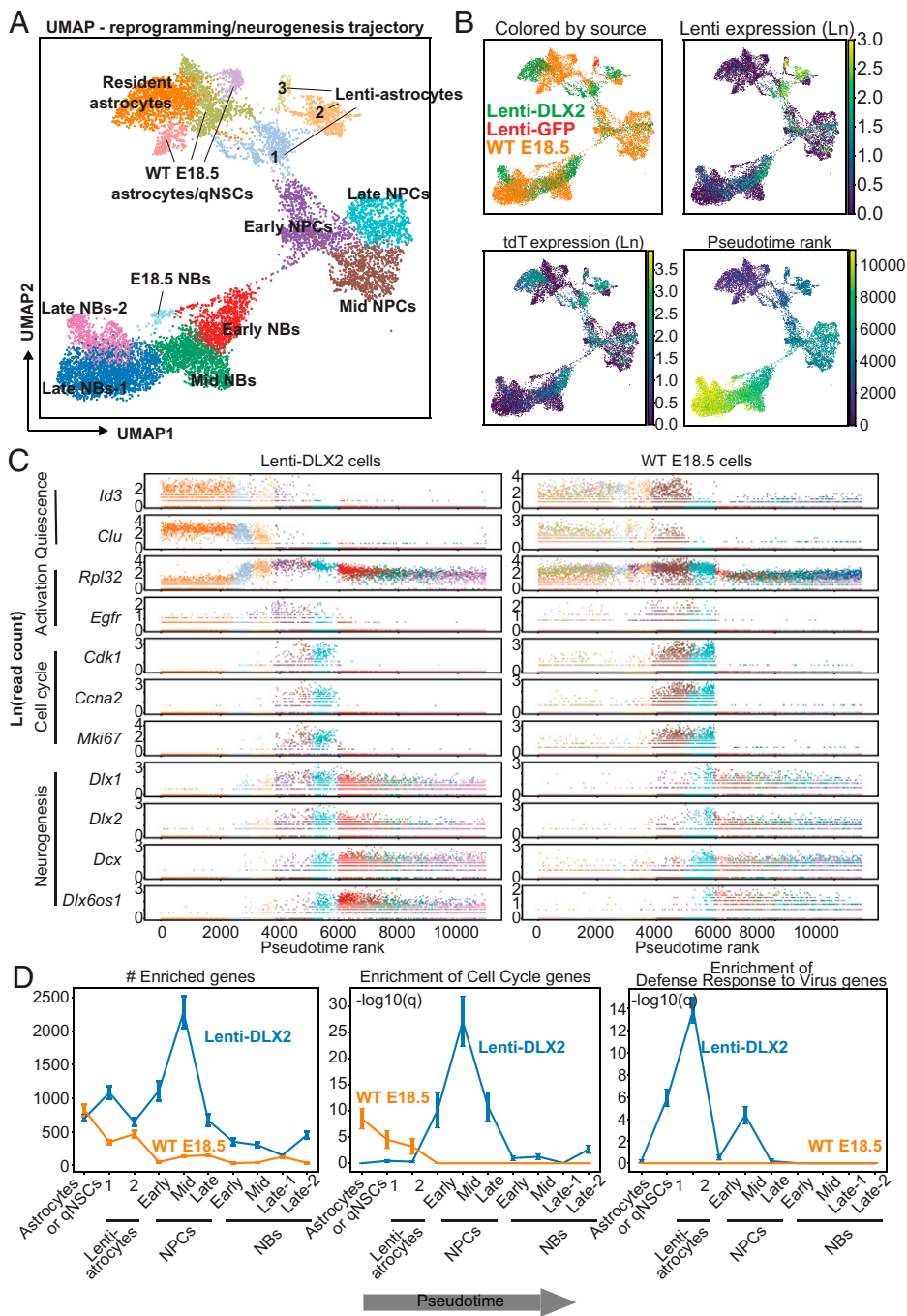


Fig. 6. scRNA-seq reveals NSC-like behaviors of reprogrammed astrocytes. (A) *Lenti-DLX2* and *Lenti-GFP* control cells are coclustered with a WT E18.5 mouse brain dataset. A sub-clustering of the main trajectory (i.e., astrocytes, lenti-astrocytes, NPCs, and neuroblasts) is shown. A Uniform Manifold Approximation and Projection (UMAP) clustering of all cell types can be found in *SI Appendix, Fig. S18B*. (B) The trajectory consists of mainly WT E18.5 and *Lenti-DLX2*, but not *Lenti-GFP* cells (Upper Left). As expected, astrocyte lineage tracer *tdT* (B, Lower Left) and lentiviral transcript (B, Upper Right) are expressed along the reprogramming trajectory. Rank of inferred pseudotime (B, Lower Right) for the reprogramming trajectory is calculated (low rank = early pseudotime). (C) In *Lenti-DLX2* cells (Left), known marker genes during adult neurogenesis in SVZ [from Dulken et al., 2017 (45)] are activated or repressed in the expected order along pseudotime, like the WT E18.5 cells (Right). (D) Differential expression analysis is performed between *Lenti-DLX2* and WT E18.5 cells at each stage of the trajectory. Though different in the first half of the trajectory, reprogramming and neurogenesis converge toward the end (D, Left). Two key differences are the expression of cell-cycle and immune-response genes (D, Center and Right).

Taken together, these analyses suggest that DLX2-induced reprogramming transcriptionally resembles endogenous neurogenesis in both adult and embryonic stages.

Discussion

The results of this study show that parenchymal astrocytes can be *in vivo* reprogrammed by a single TF into iNPCs in the adult mouse striatum. Genetic lineage tracings not only confirm the astrocyte origin, but also reveal the multilineage differentiation potential of iNPCs. The *in vivo* reprogramming process, revealed by scRNA-seq and pseudotime cell trajectories, largely resembles endogenous neurogenesis from NSCs.

scRNA-seq analysis identifies four major intermediate cell states during the early reprogramming process: astrocytes, lenti-astrocytes, NPCs, and neuroblasts. First, astrocytes can be roughly divided

into “resident astrocytes” and “astrocytes/qNSCs,” with the former exclusively from the *Lenti-DLX2* group and the latter from WT E18.5 brains. This is consistent with the fact that reprogramming starts from mature parenchymal astrocytes, whereas endogenous neurogenesis is from NSCs. Second, NPCs can be further divided into three clusters: early, mid, and late NPCs. While all express NPC markers, such as *Ascl1*, they differ in gene expression involved in the cell cycle and neurogenesis. Such results suggest that the reprogrammed cells sequentially activate NPC genes, cell-cycle genes, and neurogenesis genes. Lastly, neuroblasts can also be divided into early, mid, and late neuroblast clusters. Markers for mature neurons such as *Calb2* are increasingly expressed from early to mid to late neuroblasts, indicating that cell maturation underlies the distinction between these three neuroblast clusters.

Transient induction of *Ascl1* offers a unique opportunity to follow the fates of the reprogrammed astrocytes through genetic lineage

tracing in mice with the knockin allele of *Ascl1-CreER^{T2}*. Our time-course lineage tracing reveals that the reprogrammed astrocytes become multipotent iNPCs, giving rise to neuroblasts, neurons, astrocytes, and oligodendrocytes. Such a property of induced ASCL1⁺ cells is consistent with previous reports showing that ASCL1 marks NSCs as well as intermediate progenitors in the adult neurogenic niches (30). Although ASCL1 alone is insufficient to reprogram adult resident striatal astrocytes (48), it may be an essential mediator of DLX2 activity (17). Going forward, it will be of interest to determine the mechanism by which DLX2 induces ASCL1 expression in this reprogramming context. One possibility is that DLX2 represses the Notch pathway, which, in turn, derepresses proneural programs (13–15). Supporting this possibility is our result showing that NICD, the constitutively active form of Notch1, can suppress DLX2-mediated reprogramming. Interestingly, our staining showed that DLX2 and ASCL1 are largely localized in the same cells during the early stage of reprogramming, suggesting that DLX2 directly or indirectly (through Notch suppression) induces ASCL1 expression in a cell-autonomous manner.

DLX2-induced reprogramming strikingly mirrors the regulation of key genes during adult neurogenesis in the SVZ and the hippocampus (45, 46). In contrast, E18.5 neurogenesis has notable differences: Quiescence genes (e.g., *Clu*) are partially silenced, and activation genes (e.g., *Rpl32*) are partially activated in the beginning of the trajectory. Therefore, DLX2-induced reprogramming seems to resemble adult neurogenesis more than E18.5 neurogenesis. One possible explanation for this observation is that we performed reprogramming in the adult mouse brain. Thus, insights into adult neurogenesis can help further the understanding of cell reprogramming.

The reconfiguration of gene regulatory networks reveals metabolic switching and immune responses during reprogramming. Astrocytes use glycolysis, whereas neurons use oxidative phosphorylation, as the main energy source (38). Accordingly, genes involved in the mitochondrial respiratory chain and oxidative phosphorylation are expressed in early NPC states (cluster 3), supporting that metabolism is a potential driving force and can be harnessed for reprogramming (8). Consistently, known metabolic regulators, such as *Foxk2*, *Ppara*, *Epas1*, and *Srebf1*, are activated during reprogramming. Our analysis also shows that immune-response-related genes (cluster 10) are dynamically regulated during the reprogramming progress. Upon down-regulation of astrocyte genes (clusters 0 and 5), cluster 10 genes are up-regulated in the reprogramming initiation stage, but down-regulated quickly as cells enter the NPC stage. Although it is well known that astrocytes can be fast-activated in response to infections and injuries within 2 d (49, 50), such responses are unlikely the cause for the changes on immune-response-related genes, since our scRNA-seq analysis was performed 4 wpv, a time point that should not acutely reflect the immune-response activation. Alternatively, astrocytes as antigen-presenting cells in the CNS might need to change their immunological function once converted to neurons (51). It is highly possible that regulation of immune genes may actively contribute to the reprogramming process. As such, DLX2-induced reprogramming is not only neurogenesis/gliogenesis, but also a continuous and precise process involving the temporal regulation of metabolism and immunological events. The potential cross-talks among them require further investigation.

Of note, it was previously claimed that adeno-associated virus (AAV)-mediated expression of DLX2, when combined with NEUROD1, could efficiently convert striatal astrocytes into medium spiny neurons (52). However, such a claim was purely based on the virus-expressed reporter and couldn't be confirmed by the more stringent genetic lineage-tracing methods (11). Leaky expression of

the viral reporter in preexisting neurons accounted for what was claimed to be converted from resident astrocytes (11). Such leaky neuronal expression of the viral reporter was also observed for lentivirus-mediated expression (12). In contrast, in this study, we have systematically examined each step of the reprogramming process through genetic lineage tracings. Such a thorough analysis unexpectedly revealed multipotentiality of the lentiviral DLX2-reprogrammed astrocytes. An unresolved question is why astrocyte reprogramming was not observed when employing the AAV system (11). One possibility might be AAV-induced cell toxicity (53). It was recently shown that AAV caused rapid and persistent death of NPCs and immature neurons. Another possibility might be the differential cellular responses induced by the DNA virus AAV and the RNA virus lentivirus. These virus-induced cellular responses might contribute to fate reprogramming in vivo. Future studies are clearly required to understand the molecular mechanisms underpinning the in vivo reprogramming process.

It is long known that radial glia in the adult neurogenic niches are NSCs, whereas resident parenchymal astrocytes do not have such a property (1, 54, 55). Our study identifies a genetic switch that can turn on the latent multipotentiality of mature parenchymal astrocytes, underscoring their extreme plasticity and a potential for providing all neural cell types that are needed for regenerative medicine.

Materials and Methods

WT and mutant mice were purchased from the Jackson Laboratory. Animal procedures and protocols were approved by the Institutional Animal Care and Use Committee at the University of Texas (UT) Southwestern Medical Center. Details on animals are included in *SI Appendix*. *SI Appendix* also includes detailed materials and methods, including Tam and BrdU administration, virus preparation and intracranial injections, immunohistochemistry, single-cell isolation, 10× genomics scRNA-seq procedure and bioinformatics, and statistical analysis.

Data Availability. The scRNA-seq datasets generated in this work can be accessed through the Gene Expression Omnibus database (GSE154213). Code for scRNA-seq analyses can be accessed through GitHub (<https://github.com/liboxun/A-single-factor-elicits-multilineage-reprogramming-of-astrocytes-in-the-adult-mouse-striatum>). All other data are included in the article and/or supporting information. Materials generated in this study are available upon request.

ACKNOWLEDGMENTS. We thank members of the C.-L.Z. and G.C.H. laboratories for discussions and reagents. C.-L.Z. is a W. W. Caruth, Jr. Scholar in Biomedical Research. The work in the C.-L.Z. laboratory was supported by the Welch Foundation (I-1724); the Dechard Foundation; the Texas Alzheimer's Research and Care Consortium (TARCC2020); the Kent Waldrep Foundation Center for Basic Research on Nerve Growth and Regeneration; and NIH Grants NS099073, NS092616, NS111776, NS117065, and NS088095. The work in the G.C.H. laboratory was supported by the Cancer Prevention Research Institute of Texas (RR140023 and RP190451); NIH Grants DP2GM128203 and UM1HG011996; the Department of Defense (PR172060); the Welch Foundation (I-1926-20170325); the Burroughs Wellcome Fund (1019804); the Harold C. Simmons Comprehensive Cancer Center; and the Green Center for Reproductive Biology. We also acknowledge the UT Southwestern McDermott Center for providing sequencing service and BioHPC for providing high-performance computing and storage resources.

Author affiliations: ^aDepartment of Molecular Biology, University of Texas Southwestern Medical Center, Dallas, TX 75390; ^bHamon Center for Regenerative Science and Medicine, University of Texas Southwestern Medical Center, Dallas, TX 75390; ^cCecil H. and Ida Green Center for Reproductive Biology Sciences, University of Texas Southwestern Medical Center, Dallas, TX 75390; ^dDepartment of Obstetrics and Gynecology, University of Texas Southwestern Medical Center, Dallas, TX 75390; ^eLyda Hill Department of Bioinformatics, University of Texas Southwestern Medical Center, Dallas, TX 75390; and ^fDepartment of Pathology, University of Texas Southwestern Medical Center, Dallas, TX 75390

1. A. Kriegstein, A. Alvarez-Buylla, The glial nature of embryonic and adult neural stem cells. *Annu. Rev. Neurosci.* **32**, 149–184 (2009).
2. J. T. Gonçalves, S. T. Schafer, F. H. Gage, Adult neurogenesis in the hippocampus: From stem cells to behavior. *Cell* **167**, 897–914 (2016).
3. M. Götz, M. Nakafuku, D. Petrik, Neurogenesis in the developing and adult brain—similarities and key differences. *Cold Spring Harb. Perspect. Biol.* **8**, a018853 (2016).
4. P. M. Lledo, M. Alonso, M. S. Grubb, Adult neurogenesis and functional plasticity in neuronal circuits. *Nat. Rev. Neurosci.* **7**, 179–193 (2006).
5. C. L. Zhang, Y. Zou, W. He, F. H. Gage, R. M. Evans, A role for adult TLX-positive neural stem cells in learning and behaviour. *Nature* **451**, 1004–1007 (2008).
6. R. A. Barker, M. Götz, M. Parmar, New approaches for brain repair—from rescue to reprogramming. *Nature* **557**, 329–334 (2018).
7. W. Tai, X. M. Xu, C. L. Zhang, Regeneration through *in vivo* cell fate reprogramming for neural repair. *Front. Cell. Neurosci.* **14**, 107 (2020).
8. S. Gascón, G. Masserdotti, G. L. Russo, M. Götz, Direct neuronal reprogramming: Achievements, hurdles, and new roads to success. *Cell Stem Cell* **21**, 18–34 (2017).
9. L.-L. Wang, C.-L. Zhang, Engineering new neurons: *In vivo* reprogramming in mammalian brain and spinal cord. *Cell Tissue Res.* **371**, 201–212 (2018).
10. L.-L. Wang, C. S. Garcia, X. Zhong, S. Ma, C.-L. Zhang, Rapid and efficient *in vivo* astrocyte-to-neuron conversion with regional identity and connectivity? bioRxiv [Preprint] (2020). <https://www.biorxiv.org/content/10.1101/2020.08.16.253195v1> (Accessed 30 August 2020).
11. L.-L. Wang *et al.*, Revisiting astrocyte to neuron conversion with lineage tracing *in vivo*. *Cell* **184**, 5465–5481 (2021).
12. Y. Rao *et al.*, NeuroD1 induces microglial apoptosis and cannot induce microglia-to-neuron cross-lineage reprogramming. *Neuron* **109**, 4094–4108 (2021).
13. J. P. Magnusson *et al.*, A latent neurogenic program in astrocytes regulated by Notch signaling in the mouse. *Science* **346**, 237–241 (2014).
14. J. P. Magnusson *et al.*, Activation of a neural stem cell transcriptional program in parenchymal astrocytes. *eLife* **9**, 9 (2020).
15. M. Zamboni, E. Llorens-Bobadilla, J. P. Magnusson, J. Frisén, A widespread neurogenic potential of neocortical astrocytes is induced by injury. *Cell Stem Cell* **27**, 605–617 (2020).
16. G. Nato *et al.*, Striatal astrocytes produce neuroblasts in an excitotoxic model of Huntington's disease. *Development* **142**, 840–845 (2015).
17. W. Niu *et al.*, SOX2 reprograms resident astrocytes into neural progenitors in the adult brain. *Stem Cell Reports* **4**, 780–794 (2015).
18. W. Niu *et al.*, *In vivo* reprogramming of astrocytes to neuroblasts in the adult brain. *Nat. Cell Biol.* **15**, 1164–1175 (2013).
19. O. Torper *et al.*, Generation of induced neurons via direct conversion *in vivo*. *Proc. Natl. Acad. Sci. U.S.A.* **110**, 7038–7043 (2013).
20. A. Grande *et al.*, Environmental impact on direct neuronal reprogramming *in vivo* in the adult brain. *Nat. Commun.* **4**, 2373 (2013).
21. C. Heinrich *et al.*, Sox2-mediated conversion of NG2 glia into induced neurons in the injured adult cerebral cortex. *Stem Cell Reports* **3**, 1000–1014 (2014).
22. W. Tai *et al.*, *In vivo* reprogramming of NG2 glia enables adult neurogenesis and functional recovery following spinal cord injury. *Cell Stem Cell* **28**, 923–937 (2021).
23. Z. Su, W. Niu, M. L. Liu, Y. Zou, C. L. Zhang, *In vivo* conversion of astrocytes to neurons in the injured adult spinal cord. *Nat. Commun.* **5**, 3338 (2014).
24. N. L. Jorstad *et al.*, Stimulation of functional neuronal regeneration from Müller glia in adult mice. *Nature* **548**, 103–107 (2017).
25. T. Hoang *et al.*, Gene regulatory networks controlling vertebrate retinal regeneration. *Science* **370**, eaab8598 (2020).
26. S. Gascón *et al.*, Identification and successful negotiation of a metabolic checkpoint in direct neuronal reprogramming. *Cell Stem Cell* **18**, 396–409 (2016).
27. C. Lentini *et al.*, Reprogramming reactive glia into interneurons reduces chronic seizure activity in a mouse model of mesial temporal lobe epilepsy. *Cell Stem Cell* **28**, 2104–2121.e10 (2021).
28. R. Srivivasan *et al.*, New transgenic mouse lines for selectively targeting astrocytes and studying calcium signals in astrocyte processes *in situ* and *in vivo*. *Neuron* **92**, 1181–1195 (2016).
29. N. Kaneko *et al.*, New neurons use Slit-Robo signaling to migrate through the glial meshwork and approach a lesion for functional regeneration. *Sci. Adv.* **4**, eaav0618 (2018).
30. E. J. Kim, J. L. Ables, L. K. Dickel, A. J. Eisch, J. E. Johnson, Ascl1 (Mash1) defines cells with long-term neurogenic potential in subgranular and subventricular zones in adult mouse brain. *PLoS One* **6**, e18472 (2011).
31. L. L. Wang *et al.*, The p53 pathway controls SOX2-mediated reprogramming in the adult mouse spinal cord. *Cell Rep.* **17**, 891–903 (2016).
32. P. Arlotta, B. J. Molyneaux, D. Jabaudon, Y. Yoshida, J. D. Macklis, Ctip2 controls the differentiation of medium spiny neurons and the establishment of the cellular architecture of the striatum. *J. Neurosci.* **28**, 622–632 (2008).
33. A. V. Revishchin, V. E. Okhotin, L. I. Korochkin, G. V. Pavlova, A new population of calretinin-positive cells, presumptively neurons, with polymorphous spines in the mouse forebrain. *Neurosci. Behav. Physiol.* **40**, 541–552 (2010).
34. I. Korsunsky *et al.*, Fast, sensitive and accurate integration of single-cell data with Harmony. *Nat. Methods* **16**, 1289–1296 (2019).
35. F. A. Wolf *et al.*, PAGA: Graph abstraction reconciles clustering with trajectory inference through a topology preserving map of single cells. *Genome Biol.* **20**, 59 (2019).
36. L. Haghverdi, M. Büttner, F. A. Wolf, F. Büttner, F. J. Theis, Diffusion pseudotime robustly reconstructs lineage branching. *Nat. Methods* **13**, 845–848 (2016).
37. S. Lindtner *et al.*, Genomic resolution of DLX-orchestrated transcriptional circuits driving development of forebrain GABAergic neurons. *Cell Rep.* **28**, 2048–2063 (2019).
38. C. Maffezzini, J. Calvo-Garrido, A. Wredenberg, C. Freyer, Metabolic regulation of neurodifferentiation in the adult brain. *Cell. Mol. Life Sci.* **77**, 2483–2496 (2020).
39. B. Van de Sande *et al.*, A scalable SCENIC workflow for single-cell gene regulatory network analysis. *Nat. Protoc.* **15**, 2247–2276 (2020).
40. T. Nakatani, Y. Minaki, M. Kumai, Y. Ono, Helt determines GABAergic over glutamatergic neuronal fate by repressing NGN genes in the developing mesencephalon. *Development* **134**, 2783–2793 (2007).
41. M. Yoon, The role of PPARalpha in lipid metabolism and obesity: Focusing on the effects of estrogen on PPARalpha actions. *Pharmacol. Res.* **60**, 151–159 (2009).
42. D. Eberlé, B. Hegarty, P. Bossard, P. Ferré, F. Fufelle, SREBP transcription factors: Master regulators of lipid homeostasis. *Biochimie* **86**, 839–848 (2004).
43. J. A. Shavit *et al.*, Impaired megakaryopoiesis and behavioral defects in mafG-null mutant mice. *Genes Dev.* **12**, 2164–2174 (1998).
44. J. K. Liu, I. Ghattas, S. Liu, S. Chen, J. L. Rubenstein, Dlx genes encode DNA-binding proteins that are expressed in an overlapping and sequential pattern during basal ganglia differentiation. *Dev. Dyn.* **210**, 498–512 (1997).
45. B. W. Dulken, D. S. Leeman, S. C. Boutet, K. Hebestreit, A. Brunet, Single-cell transcriptomic analysis defines heterogeneity and transcriptional dynamics in the adult neural stem cell lineage. *Cell Rep.* **18**, 777–790 (2017).
46. J. Shin *et al.*, Single-cell RNA-Seq with waterfall reveals molecular cascades underlying adult neurogenesis. *Cell Stem Cell* **17**, 360–372 (2015).
47. H. Hochgerner, A. Zeisel, P. Lönnerberg, S. Linnarsson, Conserved properties of dentate gyrus neurogenesis across postnatal development revealed by single-cell RNA sequencing. *Nat. Neurosci.* **21**, 290–299 (2018).
48. M. M. Islam *et al.*, Enhancer analysis unveils genetic interactions between TLX and SOX2 in neural stem cells and *in vivo* reprogramming. *Stem Cell Reports* **5**, 805–815 (2015).
49. J. V. Kim, M. L. Dustin, Innate response to focal necrotic injury inside the blood-brain barrier. *J. Immunol.* **177**, 5269–5277 (2006).
50. L. Rinaman, J. P. Card, L. W. Enquist, Spatiotemporal responses of astrocytes, ramified microglia, and brain macrophages to central neuronal infection with pseudorabies virus. *J. Neurosci.* **13**, 685–702 (1993).
51. Y. Dong, E. N. Benveniste, Immune function of astrocytes. *Glia* **36**, 180–190 (2001).
52. Z. Wu *et al.*, Gene therapy conversion of striatal astrocytes into GABAergic neurons in mouse models of Huntington's disease. *Nat. Commun.* **11**, 1105 (2020).
53. S. Johnston *et al.*, AAV ablates neurogenesis in the adult murine hippocampus. *eLife* **10**, 10 (2021).
54. F. Doetsch, I. Caillé, D. A. Lim, J. M. García-Verdugo, A. Alvarez-Buylla, Subventricular zone astrocytes are neural stem cells in the adult mammalian brain. *Cell* **97**, 703–716 (1999).
55. S. Robel, B. Berninger, M. Götz, The stem cell potential of glia: Lessons from reactive gliosis. *Nat. Rev. Neurosci.* **12**, 88–104 (2011).